Archaeometry **48**, 1 (2006) 77–96. Printed in Singapore

NON-DESTRUCTIVE INVESTIGATION OF BRONZE ARTEFACTS FROM THE MARCHES NATIONAL MUSEUM OF ARCHAEOLOGY USING NEUTRON DIFFRACTION*

S. SIANO† and L. BARTOLI

Istituto di Fisica Applicata 'Nello Carrara'—CNR, Via Madonna del Piano snc (ed. C), 50019 Sesto Fiorentino, Italy

J. R. SANTISTEBAN, W. KOCKELMANN and M. R. DAYMOND

ISIS Neutron Facility, Rutherford Appleton Laboratory, Chilton, OX11 0QX, UK

M. MICCIO

Soprintendenza per i Beni Archeologici della Toscana, Largo il Boschetto 3, 50100 Firenze, Italy

and G. DE MARINIS

Soprintendenza per i Beni Archeologici delle Marche, via Birarelli, 18—60121 Ancona, Italy

Non-destructive neutron diffraction techniques were applied to determine composition and microstructure data, and hence to derive information on manufacturing techniques of Picenum bronze artefacts. Furthermore, texture analyses were carried out on standards and suitable ancient artefacts to investigate their potential role in archaeometallurgical studies. This is a first step towards an overall characterization of the bronze collection of the Marches National Museum of Archaeology, Italy, and the analytical demonstration of relations with and differences compared to Etruscan metallurgy. The work is also an example application of the powerful non-destructive archaeometrical approaches provided by time-of-flight neutron diffraction.

KEYWORDS: PICENAN BRONZES, NEUTRON DIFFRACTION, TEXTURE ANALYSIS, RESIDUAL STRESSES

INTRODUCTION

The scientific discussion regarding the use of neutron diffraction (ND) techniques in non-destructive archaeometrical studies started about five years ago with the first experimentation carried out on archaeological ceramics (Kockelmann *et al*. 2000, 2001). Since then, preliminary studies have also been performed on metals (Siano *et al*. 2002, 2003, 2004; Artioli *et al*. 2003) and marbles (Coppola *et al*. 2002). These works have clearly demonstrated the potential associated with the deep penetration (up to several centimetres) of thermal neutrons and the absence of invasive effects. In particular, such features provide significant advantages with

*Received 7 February 2005; accepted 12 May 2005.
†Corresponding author: Dr Salvatore Siano, Istituto di Fisica Applicata 'Nello Carrara'—CNR, Sede: Elettronica Quantistica, Via Madonna del Piano snc, 50019 Sesto Fiorentino, Italy. Tel. +39-055-5225310; fax +39-055-5225305; email S.Siano@ifac.cnr.it

respect to XRD whenever the objective of the investigation is a quantitative analysis of the bulk. Actually, the large probed volume (from cubic millimetres to several cubic centimetres) guarantees a high signal-to-noise ratio and meaningful statistics of the diffraction data, since in many cases of interest the probed volume contains numbers of the order of thousands to millions of crystallites. Conversely, the low spatial and analytical resolution due to the low fluxes (many orders of magnitude lower than synchrotron radiation sources) and the low scattering coefficients (around one order of magnitude less than X-rays), prevent ND from being used in stratigraphic and trace analyses.

On the basis of what has been carried out up to now, it appears that the most significant application is in the technological investigation of metals, where the main analytical tasks are the quantification of the predominant phases, the preferred orientation distributions of crystallites and the identification of residual stresses due to cold working. Depending on the neutron source (continuous or pulsed) and the diffractometer geometry, different experimental and analytical procedures could be employed to achieve such a set of information, which provides a kind of quantitative pseudo-metallography.

We are carrying out a systematic investigation of the use of time-of-flight neutron diffraction (TOF-ND) in the analysis of bronze artefacts at the neutron spallation source ISIS (Rutherford Appleton Laboratory, UK). The first characterization experiment on a couple of Etruscan objects and a set of binary bronze standards (90–10), carried out on the ROTAX multipurpose powder diffractometer, provided bronze composition analyses and mineral phase quantifications by Rietveld refinement (Rietveld 1969) and qualitative information on mechanical and thermal treatments by peak shape analysis (Siano *et al*. 2002). Our next step was aimed mainly at verifying the reliability of the quantitative analysis; at improving the determination of the tin content from the lattice parameter by deriving a calibration curve from 12 homogenized binary specimens ($A_{I–XII}$); at analysing reflection peak features of raw casting on a further 12 specimens with the same composition ($A_{1–12}$); and at improving the qualitative characterization of mechanical and thermal treatments by peak shape analysis of 10 processed specimens. The optimized phase analysis and microstructural characterization were then successfully applied to a second set of Etruscan bronzes (Siano *et al*. 2003, 2004).

At that point, we focused our efforts on the quantitative statistical analysis of preferred orientations of crystallites within the bulk (texture analysis) and on the measurement of residual stress profiles and maps, since both of them can represent fingerprints of the working history of the alloy. As is well known, casting and typical working processes such as lamination and subsequent annealing are expected to produce, for a given lattice structure, specific orientation distributions and associated pole figures (Kocks *et al*. 1998; Wenk and van Houtte 2004), while stress mapping can allow the assessment and reconstruction of the plastic deformation history of the artefact (Daymond *et al*. 1997).

The core of the present work is a non-destructive archaeometallurgical characterization of a set of bronze artefacts from the Marches National Museum of Archaeology, Ancona, Italy, based on TOF-ND techniques. The objects, attributed to local Villanovan, Picenan or Etruscan civilisations, are representative of different production routes and related technological problems. From a general standpoint, the investigation was mainly aimed at collecting data on Picenum metallurgical products. Phase quantification and qualitative microstructural characterization were achieved through experimental and analytical procedures previously developed on the ROTAX diffractometer (Siano *et al*. 2002). Residual stress mapping based on spatially resolved measurements provided by the ENGIN-X diffractometer was applied here for the first time to archaeological artefacts. For this reason, a detailed presentation of this latter technique

is provided in what follows. At the same time, the paper reports insights into texture analysis by TOF-ND performed on a set of specimens and two more ancient artefacts. The results of this methodological part are important for a thorough discussion of the present results, and for a better understanding of the possible exploitation of preferred orientation distribution analyses in technological studies. Thus, along with the successful non-destructive characterization of the bronze artefacts investigated here, we also provide a rather complete picture of the potential of TOF-ND in archaeometallurgy.

MATERIALS AND METHODS

Archaeological artefacts

Five of the archaeological objects that we studied are shown in Figure 1, along with a couple of 3-D details. These artefacts, exhibited at the Marches National Museum of Archaeology, Ancona, had not undergone any analytical investigation prior to the present one. The available archaeological data are summarized in Table 1 (G. Baldelli pers. comm., 2004). Such objects were selected as being representative of specific characterization problems. Thus, in some respects, the crystallographic study of the leach-type fibula, which represents an example situation for TOF-ND phase analysis, was aimed at comparing this possible local product with similar artefacts from other areas. The fabrication technique of this fibula typology, which was widely distributed in central Italy after the first quarter of the eight century BC, was described as lost wax. Actually, the presence of a core nail was revealed by radiographic investigations and the casting core was found in some broken samples (Babbi 2003; Rossi 2003). The present fibula exhibits an advanced state of mineralization, but details of its shape are still well preserved. Two irregularities can be observed in the central zone of the internal and external sides of the arch, which suggest that it could still contain the internal segment of the core nail and the core itself. Thus, the TOF-ND phase and microstructure analyses were very attractive

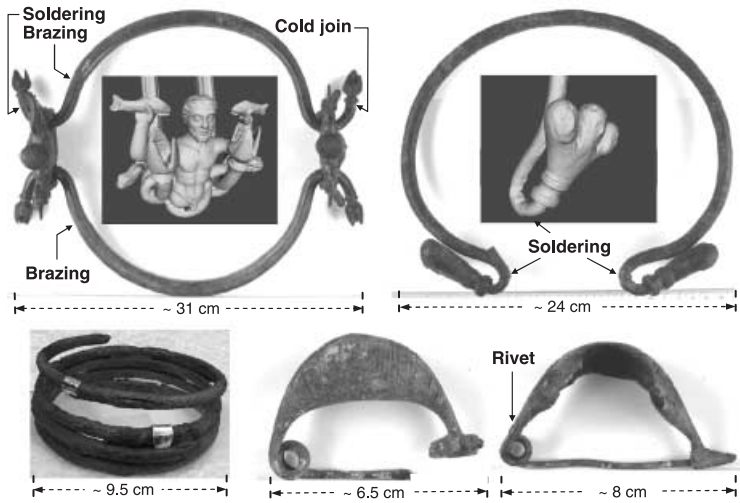

Figure 1 *The objects under investigation, from the Marches National Museum of Archaeology, Ancona.*

here in order to simultaneously characterize the arch wall, nail and core. The *navicella* fibula, which represents the direct evolution of the leach type, comes from the same archaeological site and period as the previous one. It was hence selected in order to compare the alloy and microstructure of the two fibulas.

Similar characterizations were performed on the bracelet, which represents another objects from mass production. It is a strongly corroded bronze, with thick mineral layers concealing the metal underneath. Thus, this situation also represents a case of interest for conservation purposes, because knowledge of the degree and type of mineralization is of importance in deciding whether or not to approach the restoration and, if so, in which way.

The *situla* (bucket) double handle and the *torques* (necklace) are unique artefacts in the Museum's collection. They were included in the present study mainly for the purpose of residual stress measurements. The former is composed of two bent bars terminated by four lotus flowers and two triton figures, as attachments. The *torques* is a bent bar terminated by relatively smaller sculptural elements representing three heads (Fig. 1). The two bars of the handle are slightly thicker (9–13 mm) than the ring of the necklace (7–11 mm), but they present similar shapes. The analyses were aimed at characterizing the composition of the alloys, distinguishing between raw casting and processed material, and assessing the presence of residual stresses caused by cold working. Patterns were also acquired in several specific zones in order to collect any objective attribution datum. Actually, despite the tomb where the handle was found in 1884 was identified as Gallic, the stylistic study leading to its being classified as a product from an Etruscan workshop (Baldelli pers. comm., 2004). A number of measurements were hence carried out on this artefact using both the ROTAX and the ENGIN-X diffractometers.

All of the objects were preliminarily investigated by X-ray radiography in order to better identify zones of major interest and to plan suitable TOF-ND measurements.

Texture samples

Previously reported results (Siano *et al.* 2002, 2003) on a number of standards provided reference information to analyse the patterns associated with the bronze artefacts in terms of composition and working processes. Among these, the specimens A_{1-12} mentioned above were cast in a cast iron ingot mould (32×67 mm^2, planar sizes) and then milled to a standard thickness of 7 mm in order to remove any irregularities and other boundary effects. For the purposes of this work, we produced two subsets from A_4 (Cu 96%, Sn 4%) and A_5 (Cu 94%, Sn 6%) standards, which were cut into smaller pieces to investigate the effect on texture produced by hardening and annealing cycles. A_{41}, A_{42}, A_{43} and A_{44}, from the raw casting A_4, were hammered up to thickness reductions of 7.9%, 19.3%, 30.7% and 45.7%, respectively. The texture analysis of these specimens was aimed at achieving and verifying the pole figure associated with the most common cold working of the past; that is, hammering. The second subset, A_5, A_{5h}, A_{5ha} and A_{5hah}, which included a raw casting, and hardened (21.4%) and annealed (20 min at 700°C) specimens, according with the reported indexes (h and a), was used to test the effect on texture of complex material processing. This systematic approach was performed here in order to understand the nature of the weak texture effects associated with the objects investigated, as well as for more general purposes. In this methodological framework, two archaeological bronze artefacts with a simple planar geometry were also selected as example cases for quantitative texture analysis. They were a late Etruscan mirror and a Roman coin (Table 1) from the National Museum of Archaeology, Chiusi (Siena) and the Roman site of Vada (Pisa).

Table 1 *The available archaeological data on the investigated bronze artefacts*

Artefact (Museum, catalogue number)	*Find site, date*	*Chronology*	*Production area*
Leach-type fibula (MNMA, 19843)	Villanovan necropolis, Fermo (Ascoli Piceno), 1956	Second half of the eighth century BC	Local or central Italy
Navicella fibula (MNMA, 19845)	Villanovan necropolis Fermo (Ascoli Piceno), 1956	Second half of the eighth century BC	Local or central Italy
Bracelet (MNMA, 495)	Picenan necropolis Torre San Patrizio (Ascoli Piceno), 1934	Sixth century BC	Local
Torques (MNMA, 10983)	Picenan necropolis Belmonte Piceno (Ascoli Piceno)	First half of the sixth century BC	Local
Double handle (MNMA, 4870)	Gallic tomb, San Ginesio (Macerata), 1884	Fourth century BC	Etruscan, or local
Mirror (NMAC, 62550)	Unknown; from the Paolozzi collection	Second century BC	Etruscan
Coin	Roman site of Vada (Pisa)	Third to seventh centuries AD	Rome

Note: MNMA, Marches National Museum of Archaeology, Ancona; NMAC, National Museum of Archaeology, Chiusi (Siena).

The experimental set-ups

Diffraction measurements for phase and texture analyses were carried out on the ROTAX diffractometer, which is equipped with three detector banks positioned at different scattering angles. The layout of this instrument can be found in Kockelmann *et al*. (2000, 2001).

Static measurement configurations and relatively long acquisition times (1–2 h) were used for phase analysis. Weight fractions in the multiphase mixture were achieved through multi-bank Rietveld refinements using the GSAS code (Larson and Von Dreele 1986), which also allowed us to take preferred orientation effects into account. As in previous works, a pure aluminium sheet surrounding the probed volume was used to correct any sample misalignment and off-axis problems during pattern refinements by providing a reference lattice parameter.

The bronze lattice parameter calculated by Rietveld refinement allows to derive the tin content in the α(Cu) phase by using the calibration curve mentioned above (Siano *et al*. 2003), which provides a sort of indirect chemical analysis of the alloy.

Experimental pole figures were measured using the backscattering detector bank (bank 3, $101° < 2\theta < 143°$) only. The (α, β) pole coverage corresponding to the angular acquisition sets is shown in Figure 2, where the normal to the surface of the investigated object is orthogonal to the pole figure plane in the cases of the standards and the coin, while it coincides with the ordinate for the mirror. Orientation distributions and associated equal area projections (reconstructed pole figures) were calculated by the code MAUD, using the EWIMV algorithm (Lutterotti *et al*. 1999).

The existence of residual stresses within the specimens was assessed using ENGIN-X, the neutron strain scanner diffractometer at ISIS (Dann *et al*. 2004). Plastic deformation introduces residual internal stresses, resulting in internal elastic strains. In essence, neutron

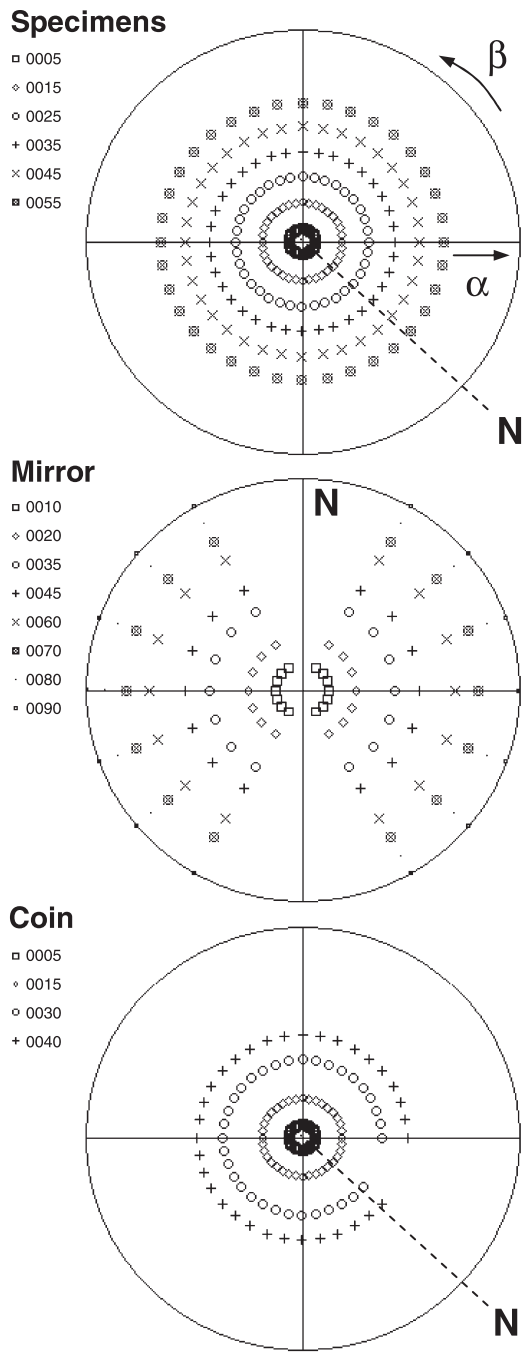

Figure 2 *Measurement of the experimental pole figures: the angular coverage used for standards (top), the Etruscan mirror (middle) and the Roman coin (bottom). N indicates the normal to the sample surface, which is orthogonal to the plane of the plots for the specimens and the coin, and parallel to the ordinate for the mirror.*

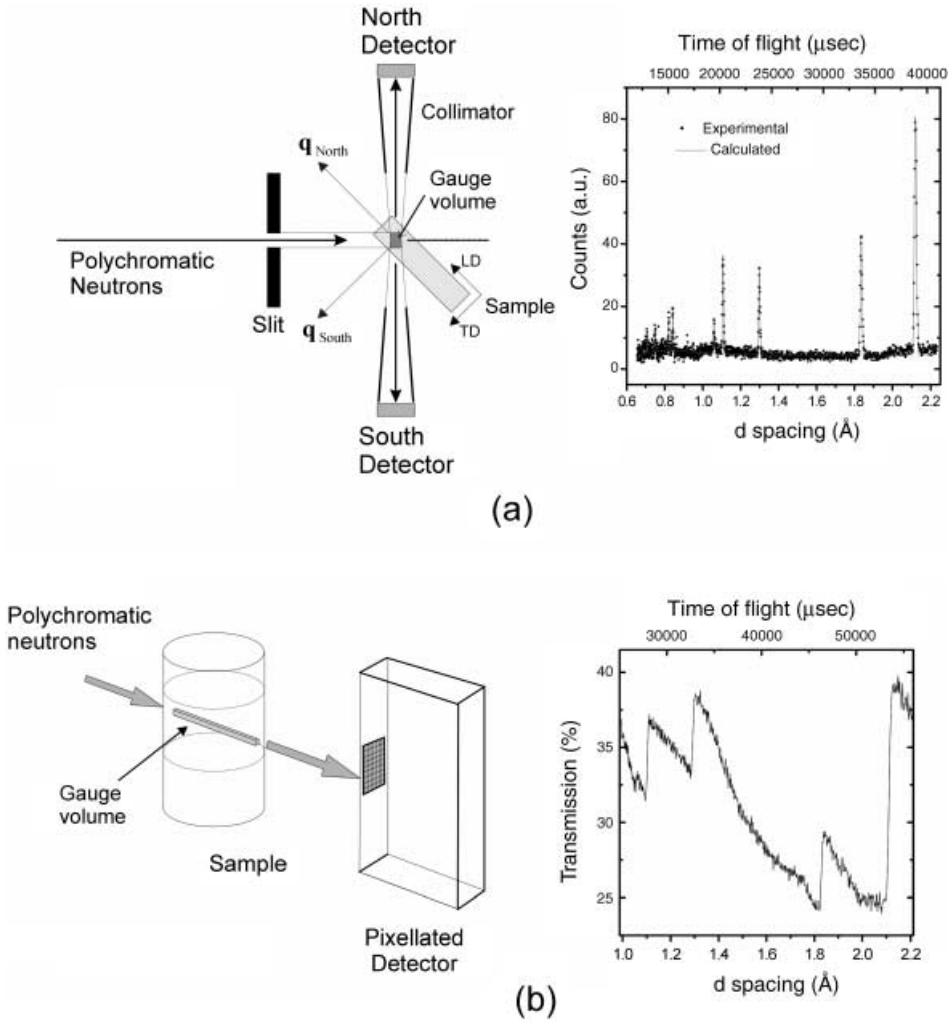

Figure 3 *The (a) diffraction and (b) transmission set-ups of the ENGIN-X diffractometer, with examples of typical patterns associated with the* torques *('powder'-like sample).*

strain scanning uses the planes of atoms as microscopic strain gauges, as elastic strain is revealed by shifts of the diffraction peaks. Two different techniques, *diffraction* and *transmission*, were used on the ENGIN-X diffractometer to investigate the necklace and the *situla* double handle.

The *diffraction* technique (Allen *et al.* 1985) is based on analysis of the spectra recorded by a detector placed at 90° to the incident beam, as is schematically shown in Figure 3 (a). In this set-up, the volume gauged by the experiment is a cuboid defined by the intersection of the incident and diffracted beams, as defined by the use of slits or collimators. In a typical experiment, the sample is moved across the beam using a positioning table, and the strain at each location is deduced from the shift observed in the diffraction peaks. The measured strain corresponds to the direction of the momentum exchange vector **q**, located at the mid-angle

between the incident and the diffracted beams, as is indicated in Figure 3 (a). Two diffraction banks (North and South) are available on the ENGIN-X diffractometer, which allows measurement of the strain along two perpendicular directions simultaneously. In the example shown in Figure 3 (a), the sample has been oriented so as to measure the longitudinal (LD) and transverse (TD) components of the strain tensor. Gauge volumes of $2 \times 2 \times 2$ mm^3 were used throughout the present experiments. Diffraction patterns were analysed by Rietveld or Pawley refinement, through the GSAS code (Rietveld 1969; Pawley 1981; Von Dreele *et al*. 1982).

The second technique measures the changes that appear in the neutron spectra transmitted by the sample (Fig. 3 (b)). The set-up is similar to that of the neutron radiography, but this technique uses a 10×10 TOF detector array of 2×2 mm^2 rather than film or a CCD camera. The neutron spectrum recorded by each pixel, which corresponds to an average through the thickness, displays sudden, well-defined increases in intensity as a function of the neutron wavelength λ. These so-called 'Bragg edges' correspond to coherent scattering by the lattice planes. These edges occur because, for a given $\{hkl\}$ family, the Bragg angle of the diffraction cone increases as the wavelength increases, until 2θ is equal to 180°. At wavelengths greater than this critical value, no scattering by this $\{hkl\}$ family can occur and there is a sudden increase in the transmitted intensity. The wavelength at which this occurs (at $\lambda = 2d_{hkl}$) provides a measure of the interplanar distances d in the direction of the incoming beam. Strain maps can be produced by measuring the shift of these Bragg edges across the specimen (Santisteban *et al*. 2002). The precise location of the edges is defined through a least-squares refinement of the data, using an edge profile that takes into account the broadening introduced by the sample and instrument resolution (Santisteban *et al*. 2001). On the other hand, the neutron spectrum transmitted by single crystals is radically different from that of polycrystalline specimens, as diffraction takes place in the form of Laue spots rather than Bragg cones. Hence, instead of Bragg edges, the transmitted neutron spectrum contains a series of dips in intensity corresponding to the neutrons diffracted into a Laue spot. So, in addition to strain analysis, a qualitative assessment of the specimen can be made on the basis of the shape of the transmitted spectrum.

RESULTS

The preliminary radiographic investigation of the leach-type fibula and the double handle provided regions of interest for the subsequent TOF-ND characterization, whereas for the other objects it did not add significant details to the visual and microscopic inspection. As shown in Figure 4, the leach fibula still contains the internal part of the core nail, which is positioned transversally to the arch, almost at the middle. Radiography did not show any evidence of core material.

The most interesting radiographic features of the double handle were two bronze brazings of similar shapes, made to join one of the terminal parts of the handle (Fig. 1). This detail is apparently of interest in understanding the manufacturing technique. Actually, the tritons (attachments) could not have been inserted through the four lotus flowers that terminate the bars, because the available holes are too small (see the 3-D detail in Fig. 1). Visual inspection and radiography also revealed various peculiarities of these flowers, suggesting possible undocumented restoration. Two of them presented regular internal cavities at the connection with the bars and a cross-cutting fracture, while the third one was tin-soldered. However, the fourth one, which did not show any evidence of modification, also presented relatively large irregular internal cavities. This suggests that the flowers were probably cast on the bent bars after insertion of the triton sculptures, whereas the two brazing joints seem unrelated to the

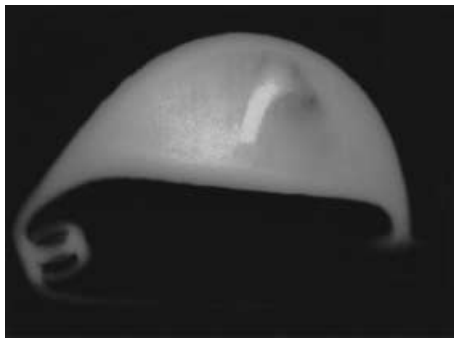

Figure 4 *Radiography of the leach-type fibula, showing the internal part of the core nail.*

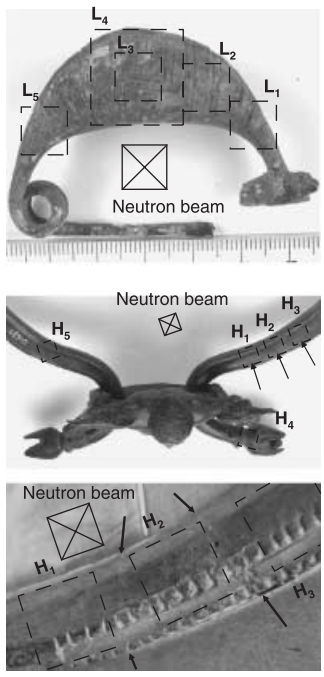

Figure 5 *The probed zones of the leach-type fibula (top) and the* situla *double handle (middle and bottom). The neutron beam is orthogonal to the plane of the pictures. Black arrows in the detail at the bottom indicate the margins of the brazing (H_2).*

specific requirements of the manufacturing technique. They probably represent repair sites and/or a case of reuse of material.

Similar preliminary investigations were performed on the other objects, where mineralization zones and evidence of recent restoration interventions were found, which were taken into account in order to select TOF-ND analysis sites. The volumes where phase analyses and residual stress scans were performed on the leach-type fibula and the double handle are shown in Figure 5.

Table 2 *Phase quantification and alloy composition as determined through the Rietveld refinement of the TOF-ND patterns and the linear dependence of the α(Cu) lattice parameter on tin content. First rows, absolute weight ratios in the probed volume; second rows, renormalized values*

Artefact	*Site (spot sizes, cm × cm)*	*Sn [wt%]*	*Cu [wt%]*	*Pb [wt%]*	*Cu_2O (CuCl) [wt%]*	*$CaCO_3$ [wt%]*	*SiO_2 [wt%]*	χ^2
Leach-type fibula	Tag edge	4.9	85.2	2.3 ± 0.3	2.2 ± 0.1	4.3 ± 0.1	1.1 ± 0.1	1.5
	L_1 (10 × 10)	5.4	92.0	2.6		79.6	20.4	
	Tag middle	6.0	79.9	2.3 ± 0.4	5.1 ± 0.2	4.7 ± 0.2	1.9 ± 0.2	1.9
	L_2 (10 × 10)	6.8	90.6	2.6		71.2	28.8	
	Middle	5.4	77.8	3.3 ± 0.5	2.9 ± 0.2	8.1 ± 0.3	2.3 ± 0.2	1.6
	L_3 (10 × 10)	6.2	90.0	3.8		77.9	22.1	
	Middle	5.1	81.2	2.0 ± 0.4	3.2 ± 0.2	6.5 ± 0.2	2.0 ± 0.2	1.7
	L_4 (20 × 20)	5.8	91.9	2.3		76.5	23.5	
	Spring edge	4.8	82.9	3.1 ± 0.4	1.7 ± 0.1	5.9 ± 0.2	1.5 ± 0.1	2.6
	L_5 (10 × 10)	5.3	91.3	3.4		79.7	20.3	
Navicella fibula	Centre	9.1	77.7	2.9 ± 0.4	10.3 ± 0.2	–	–	2.8
	N (20 × 20)	10.1	86.7	3.2				
Bracelet	Upper ring	8.4	91.6		10.2 ± 0.2	–	–	2.9
	B_1 (10 × 10)				(1.4 ± 0.5)			
	Second ring	8.4	91.6		22.3 ± 0.3	–	–	2.9
	B_2 (10 × 10)				(2.8 ± 0.1)			
Torques	Three heads	8.4	63.7	27.9 ± 0.3	–	–	–	3.9
	T_1 (5 × 5)							
	Middle	6.7	93.3		4.4 ± 0.1	–	–	1.9
	T_2 (10 × 10)							
Situla double handle	Below brazing	9.4	88.0	2.6 ± 0.5	–	–	–	3.3
	H_1 (10 × 10)							
	On brazing	7.2	84.9	7.9 ± 0.3	–	–	–	1.9
	H_2 (10 × 10)							
	Above brazing	9.6	87.8	2.6 ± 0.3	–	–	–	2.5
	H_3 (10 × 10)							
	Second brazing	6.0	83.6	10.4 ± 0.4	–	–	–	2.4
	H_5 (10 × 10)							
	Flower	8.8	90.5	0.7 ± 0.3	–	–	–	1.4
	H_4 (10 × 10)							
Mirror	Centre	13.0	87.0		3.6 ± 0.1	–	–	2.6
	M_1 (10 × 10)							
	Handle	12.6	87.4		2.6 ± 0.1	–	–	2.6
	M_2 (10 × 10)							
Coin	Centre	6.6	74.2	19.1 ± 0.1	–	–	–	4.6
	C (20 × 20)							

Phase, alloy composition and peak shape analyses

The acquired *d*-spacing spectra were analysed by the GSAS code through multi-bank Rietveld refinements, taking into account possible texture effects. Quantitative phase analysis results are summarized in Table 2, while Figure 6 displays an example of pattern refinement corresponding to the ornament of the necklace (three heads, T_1).

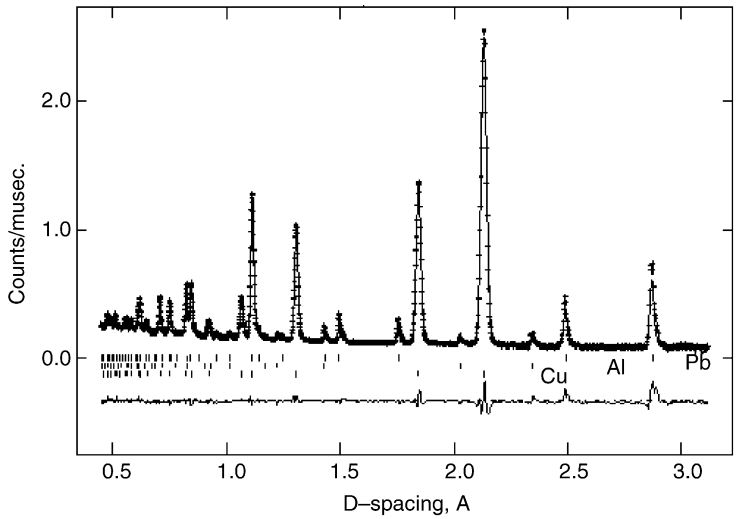

Figure 6 *An example of pattern refinement: the sculpture terminating the torques (three heads, T_1). Relatively intense lead peaks are observed along with the bronze and aluminium (reference) peaks.*

In Table 2, alloy compositions and mineral phases (expressed as percentage weight fractions, wt%) are reported in two rows. The first shows the absolute values provided by Rietveld refinement and the experimental scaling law of the lattice parameter on the previously derived tin content (Siano *et al*. 2003). The second row reports metal concentrations in the alloys and, in the case of the fibula, the relative abundance of the casting core minerals. Cuprite wt% is always reported as an absolute value in the probed volume; it can be considered as a kind of alteration index.

As can be seen, bronze with 5–7 wt% tin and a relevant amount of lead (2–4 wt%), cuprite, calcite and quartz were found in the leach fibula, where the earthy components represent the main minerals of the core. Another important datum concerning the composition of the latter was the relatively intense and structured background, which is probably associated with a non-negligible amount of organic matter. No independent diffraction contributions were associated with the core nail, which means that it has the same composition as the fibula alloy. Despite the fact that the *navicella* fibula comes from the same site and belongs to the same archaeological period as the previous one, its alloy has a higher tin content, while the lead content is similar (3 wt%). The analysis of the bracelet revealed a high degree of alteration, with a significant amount of cuprite along with a relevant fraction of nantokite, which has never before been detected in other objects investigated by TOF-ND. An intermediate tin content and the absence of lead are the characteristics of its alloy, which is similar to that of the necklace bar. In contrast, a high lead content (27.9 wt%) was found in the three head sculptures terminating the necklace. The significant lead content (7.9–10.4 wt%) found in the brazing joints of the handle is also particularly interesting, as is the agreement between the tin content of the mirror and the literature data on late Etruscan production (Cateni 1995).

As mentioned above, peak shape analysis of diffraction patterns can provide qualitative information on the metal microstructure and hence the metal processing. In a previous work (Siano *et al*. 2003), we have demonstrated that as-cast alloys are characterized by broad and

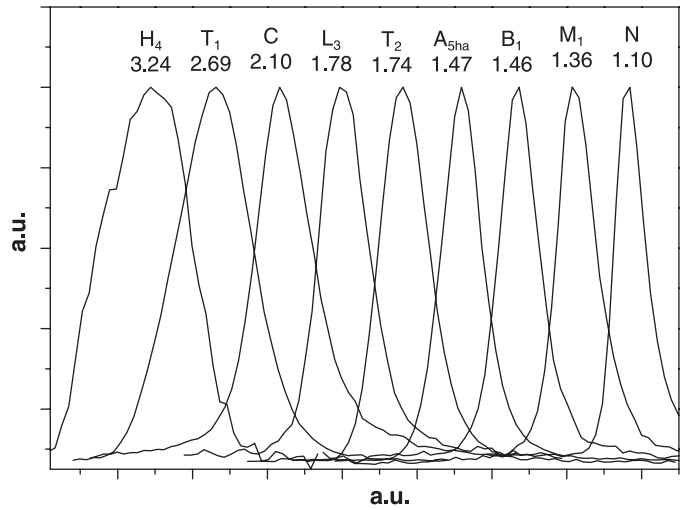

Figure 7 *Comparisons amongst the diffraction peaks and relative widths ($\Delta d/d \times 10^{-2}$) associated with the (200) lattice plane of the different objects and probed zones. The peaks are normalized to their maximum and arbitrarily shifted along the d-spacing axis. a.u., Arbitrary units. For sample abbreviations, see Table 2.*

often structured (irregular) reflection peaks due to dendritic segregation, whereas annealing and recrystallization processes produce narrow peaks. Cold working following annealing is associated with regular peaks of variable width ranging between these two limiting situations, depending on the residual stress values and distributions.

Figure 7 displays comparisons amongst the α(Cu) (200) peaks associated with the probed zones of the various objects. The (200) peak was selected because it is intense and isolated from other reflections; in particular, it is not superimposed on the eventual δ(Cu) phase peaks. All of the probed zones of the double handle, including a bar, a flower and the two brazing joints, provided broad and structured peaks, which indicates that the various parts of the object were produced by casting. Eventual pre-heating to cast the flowers and to perform the brazing joints did not produce relevant homogenization effects. The same is true for the three heads of the necklace. The smoother peak profile associated with the latter can be attributed to the relatively low solidification point and slow cooling rate caused by the lead content and the relatively large metal thickness. The coin, the arch of the fibulas, the bar of the *torques*, the bracelet and the mirror were hardened and then annealed at least once. The peak widths of the bracelet, the mirror and the *navicella* fibula are close to that of A_{5ha}, which indicates that the last treatment in their production process was an annealing stage. In the case of the bracelet, this could have been performed before bending the hardened wire, in order to avoid breaking, as well as a final treatment in order to achieve a high deformation capability, which was important for its actual use. The simplification of the final incision of the decorative motifs could justify the annealing of the *navicella* fibula and mirror.

The *torques*, the leach fibula and the coin have regular peak shapes, with widths between the two described cases of as-cast and annealed alloys. As mentioned above, this is compatible with a final hardening and/or other cold deformations. On the other hand, the present characterization approach is not unequivocal, since in principle a partial homogenization could produce similar features. This is a limitation of the present fixed-angle bulk analysis using the

ROTAX diffractometer. Unequivocal and more detailed information can be derived through scanning and mapping of microstrains using the ENGIN-X diffractometer.

Microstrains

Microstrain measurements performed at the sites H_1, H_2 (brazing) and H_3 (Fig. 5) of the double handle and at the site T_2 of the *torques* using the diffraction and transmission set-ups shown in Figure 3 provided important microstructural data. The radial scans in H_1 and H_3 revealed broad peaks with a flat top and a marked texture effect, as evidenced by irregular peak intensities. The peak intensity ratios were fairly constant throughout the scan, which indicates that the preferred orientation is the same. This behaviour is compatible with the presence of a cube texture associated with the typical columnar structure, which occurs perpendicularly to the mould surface. Conversely, as shown in Figure 8, such a feature was not present in the brazing zone H_2, where crystallites appeared to be randomly oriented. In the transmission configuration, the bronze bars of the handle displayed very distorted transmission spectra, which were composed of several 'single-crystal'-like contributions, thus confirming once again the presence of a preferred orientation, whilst the brazing presented 'normal' Bragg edges.

For the necklace, all pixels showed the characteristic Bragg edges appearing in polycrystalline specimens (the superposition of randomly oriented small crystallites), with only minor departures from an isotropic theoretical transmission (see, for example, the pattern reported in Fig. 3 (b)), which is indicative of only a very small or negligible degree of preferred orientation. A strain map of the selected region around the middle of the bar (T_2) was then calculated through the analysis of the Bragg edge shifts. As shown in Figure 9 (a), we found an inhomogeneous microstrain distribution, which is clear evidence of residual stresses originating from cold deformation of the bar during the final working step of the manufacturing. The map represents a plane projection of the microstrain distribution through the probed volume. Two microstrain

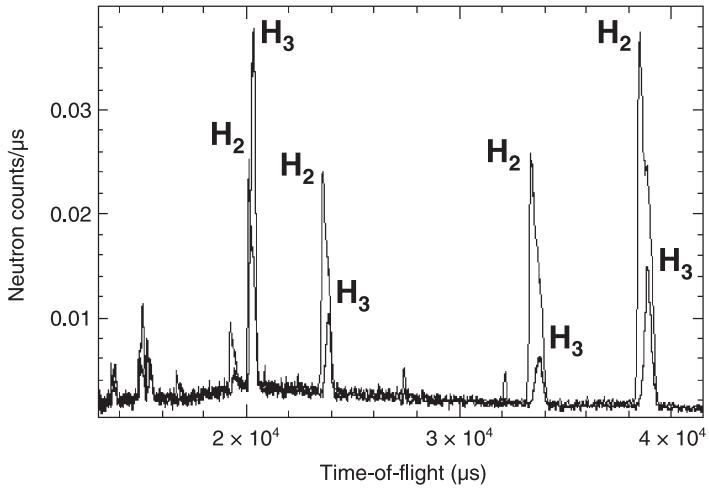

Figure 8 *The* situla *double handle: a comparison between the diffraction patterns of a brazing site (H_2), showing an almost powder-like pattern, and an adjacent zone of the bar (H_3), whose peak intensity ratios are completely different because of the preferred orientation of the crystallites.*

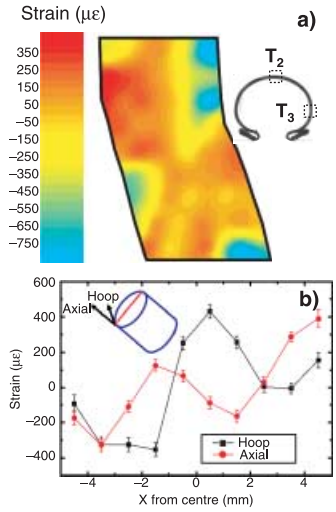

Figure 9 *Residual stresses in the necklace bar: (a) a map of the average microstrains ($\varepsilon = \Delta d/d$) through the bar (site T_2), determined by analysing the Bragg edge shifts (transmission set-up); (b) two orthogonal microstrain profiles in a lateral zone of the bar (T_3), determined by analysing the shifts of the diffraction peaks.*

profiles along orthogonal directions were also measured in a lateral zone (T_3), where the contribution of eventual plastic deformations due to use is probably negligible. The 'powder'-like spectra achieved in this case (an example is shown in Fig. 3(a)) allowed the derivation of the microstrain profiles of Figure 9 (b). Opposite double-phase modulations were observed along the axial and hoop directions, this being a typical behaviour produced by cold bending.

Texture

In the investigated set of artefacts, only the bars of the *situla* double handle exhibited relevant departures of the peak intensity ratios with respect to the expected values for random distribution, because of the cube texture associated with a columnar structure. So far, after analysing about 15 very different Villanovan, Etruscan and Picenan bronze objects, this is the only case to have shown a marked texture effect. Thus, the need to better understand such a general behaviour, along with the objective difficulties in acquiring experimental pole figures for objects with a complex geometry, such as the present ones, led us to perform a systematic investigation on standards and on two ancient artefacts with planar geometry; a mirror whose diffraction patterns did not exhibit relevant variation of the intensity ratios and a coin that showed some variations.

The reconstructed pole figures associated with the standard sets A_4 and A_5 provided useful interpretation data. As shown in Figure 10, the hammered specimens A_4 are characterized by the alignment of the pole of the (110) planes with the normal to the specimen surface. In other words, there is a statistical predominance of (110) planes that are parallel to the specimen surface. Rotation symmetry associated with hammering and the multiplicity of the reported plane sets allow the interpretation of the displayed pole figures. They represent a fibre-like texture given by a superposition of Brass $\{\bar{1}10\}<112>$ and Goss $\{110\}<001>$ components driven by

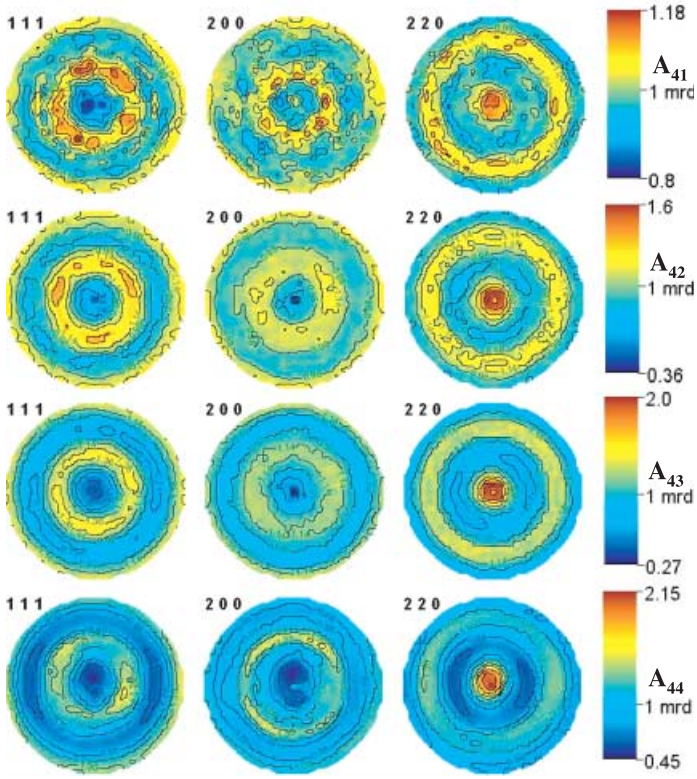

Figure 10 *The sequence of reconstructed pole figures of binary bronze standards (Cu 96 wt%, Sn 4 wt%), ordered according to an increasing degree of hardening. Relative reductions of thickness (from top to bottom): 7.9%, 19.3%, 30.7% and 45.7%.*

the dominant slip system of the fcc lattice, {111}<110>. The sequence of Figure 10 provides a quantitative evaluation of the dependence of the preferred orientation on the degree of hardening. The largest value was 2.15 mrd (multiple of random distribution), which in general represents a moderate orientation index since, in strong texture cases, a maximum can be in the order of 10 mrd. In any case, a significant variation of around a factor of two was observed in the texture parameter while stepping from a 7.9% to a 45.7% degree of hardening. This can be of practical importance in associating the texture strength with the hardening range of the artefact zones investigated.

The pole figures achieved for standard set A_5 are shown in Figure 11. Minor departures from random distribution were found for the as-cast specimen, apart from some random poles associated with large crystallites. A_{5h} returned a texture similar to that of the previous specimen set A_{4x}. The subsequent annealing (A_{5ha}) produced a randomization effect on the (110)<001> texture, as can be seen by the fragmentation, distortion and peak values (from 1.52 to 1.19), but it remains still easily visible. No new preferred orientations were produced by annealing. Finally, A_{5hah} again exhibited a fibre-like texture as above with a higher peak, but a less regular one than for A_{5h}.

Reconstructed pole figures for the two objects investigated provided examples of two opposite situations (Fig. 12). The preferred orientations were not relevant for the mirror, whereas

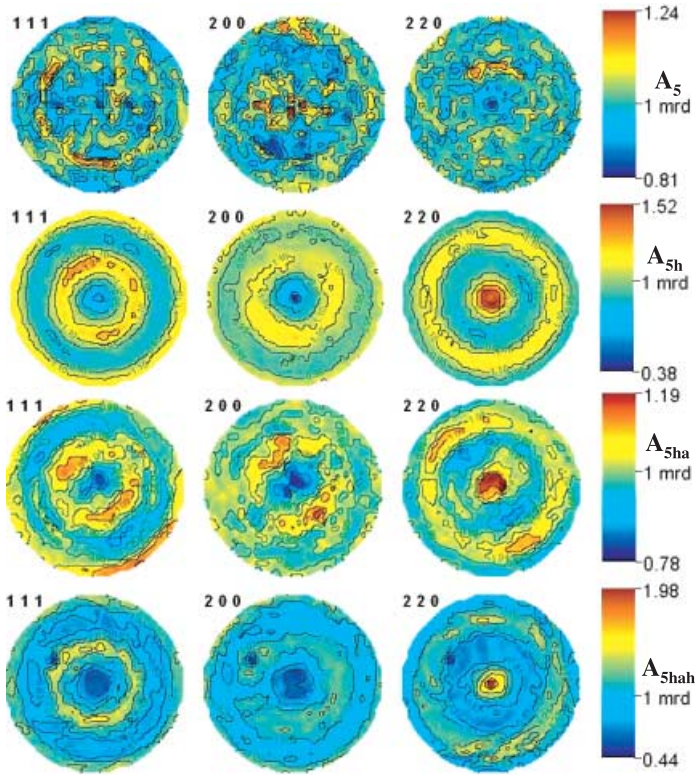

Figure 11 *The sequence of reconstructed pole figures of binary bronze standards (Cu 94 wt%, Sn 6 wt%), obtained by casting (A_5), hardening (A_{5h}), hardening plus annealing (A_{5ha}) and hardening plus annealing plus hardening (A_{5hah}).*

the coin exhibited the typical texture resulting from hammering, as previously described. The mirror pole figures also include some hot spots, which could be ghosts due to neutron absorption through long paths in the alloy bulk occurring at particular angular settings (Yanxia *et al*. 2004). The texture observed for the coin is clear evidence that the last step of its production involved striking, whereas the absence of texture in the mirror suggests that the last treatment was thermal. These conclusions are in agreement with those provided by peak shape analysis (Fig. 7).

DISCUSSION AND CONCLUSIONS

Quantitative phase analysis represents one of the main advantages of ND with respect to XRD. The ND detection limits, usually reported to be around 1%, depend on the microstructural parameters and atomic species. In our experience, we have found that the minimum detectable lead content is around 0.5%, which is also the maximum absolute error for ternary standards without marked texture effects. Despite the fact that the Rietveld refinement provides a χ^2 value that approaches 1 when the quality of the fitting increases, and the associated maximum deviations, there are no rigorous methods for error estimation in a TOF-ND multiphase analysis, mainly because of the possibility of undetected phases and the assumption of a 100% phase sum during Rietveld refinement.

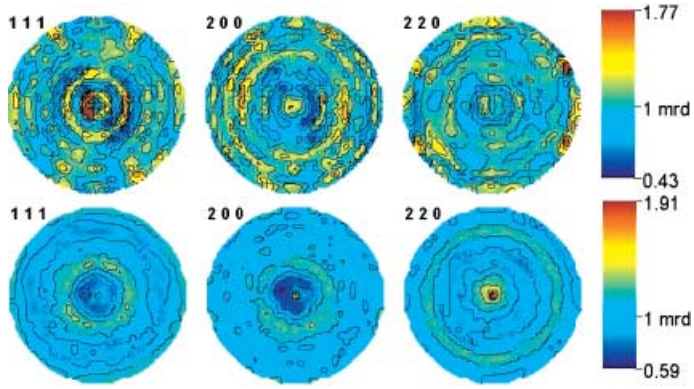

Figure 12 *Reconstructed pole figures for the Etruscan mirror (top) and the Roman coin (bottom).*

The present analyses also include the determination of the tin content through a calibration curve. Of course, this is based on the assumption of binary (Cu–Sn) bronze, without any possibility of distinguishing between different alloying metals; it can be regarded as a sort of tin-equivalent composition. The measurements carried out on binary bronze standards have, in this case, also provided maximum absolute deviations with respect to the nominal compositions within 0.5 wt%. Thus, taking into account that the data represent average values obtained from analyses of volumes of material of the order of cubic centimetres, the Rietveld refinement of TOF-ND patterns represents a relatively reliable quantification method for the weight fractions of the main metals in binary (Cu–Sn) or ternary (Cu–Sn-Pb) bronzes, as well as those of the associated alteration products.

Within the inherent analytical limits described above, the data of Table 2 allow us to draw some preliminary considerations on the set of Picenan objects investigated. Despite the different compositions, both the fibulas and the handle are characterized by similar lead contents of about 3 wt%. Such a feature was also observed in small Etruscan artefacts dated between the fifth and the second centuries BC, where a 2–5 wt% lead content was found (e.g., Pecchioli *et al*. 1989; Del Francia 1998); on the other hand, the addition of variable quantities of lead in cast objects is a well-known feature of central Italian bronze production (Craddock 1986; Riederer 1999). Conversely, lead is present only in traces in artefacts produced through several hardening and annealing cycles, such as many mirrors, thin-walled pots and vessels, and other items (Craddock 1986; Cateni 1995; Riederer 1999). This is the case for the necklace and the bracelet. Thus it seems that there is sound evidence for an intimate relationship between the present set of objects and the contemporaneous Tuscan metallurgy (Villanovan and Etruscan). Such a relation is also confirmed by the brazing technique in the double handle. In fact, the lead content was increased with respect to the bars by up to 8–10 wt% in order to have a higher fluidity and a lower solidification point during casting, in agreement with the brazing methods used by Greek and Etruscan metalworkers (Giachetti *et al*. 1984; Pecchioli *et al*. 1989; Del Francia 1998).

The scans of the handle using the ENGIN-X diffractometer showed a typical columnar structure, which is clear evidence, along with the broad Bragg peaks, that the bars were cast and did not undergo any overall thermal or mechanical treatment. The development of the columnar structure was favoured by the high tin content, which corresponds to a relatively low

solidification temperature. Conversely, the complex geometry of the brazing and its fast cooling induced by the metal contact resulted in the disordered microstructure revealed by the diffraction scan (Fig. 8). The strain map and scans for the necklace bar (Fig. 9) demonstrated that it was produced through multiple thermal and mechanical treatments, which included a final bending. This suggests that the manufacturing of such objects began with the casting of a straight rod, which was then cut and modelled to fit a given neck diameter. Unlike the bracelet, the final material is elastic rather than plastic, which is a very interesting feature.

As explained, we have included in the present study a systematic investigation on texture in order to better understand the absence of relevant preferred orientation effects for the greater part of the objects studied to date. So far, only a few non-destructive texture analyses have been carried out on archaeological objects (Artioli *et al*. 2003; Siano *et al*. 2004; Yanxia *et al*. 2004). There is a great interest in the topic because, at least in principle, crystallite orientation distributions could store a 'trace' of the various working phases. Thus, reconstructed pole figures could represent fingerprints of the whole manufacturing process. The results achieved for standards and artefacts have shown that, in practice, preferred orientations in cast objects probably occur (cube texture) when a low solidification point alloy and a low-conductivity mould were used. Apart from some statistically meaningful macro-crystallites (Fig. 11), we have not found a cube texture in the standard A_5 because of the low temperature of the oven (1100°C), the small amount of cast material (200 g) and the cast iron mould, which have favoured rapid diffuse nucleation through the material during casting, thus producing an equiaxial orientation distribution.

The texture results for the A_4 standards show that cold lamination by hammering produces a fibre-like orientation distribution, whose strength increases with the degree of hardening. The subsequent annealing does not produce a cube texture such as that appearing in copper annealing after strong lamination (Kocks *et al*. 1998) but, rather, a 'randomization effect' of the initial fibre-like texture. What we refer to as a 'randomisation effect' here should be more precisely defined by means of further tests, since complex recrystallization textures could be associated with different tin content alloys (Humphreys and Hatherly 1996). At present, if the texture observed in the standard samples A_{ha} or A_{hah} were found in an archaeological object, it would be hard to decide whether or not the piece was annealed, and at which processing stage.

The coin shows a good example of a fibre-like texture induced by hammering, which demonstrates the final striking process, but such a texture does not provide information about the preparation of the blank flan. Its preliminary hammering and annealing can be qualitatively inferred only through the peak shape analysis discussed above. The mirror, which does not show any relevant departure from random orientation distribution, represents an even more complex case. Actually, as revealed by peak shape analysis, the alloy was subjected to one or more hardening and annealing cycles, which probably 'erased' the eventual fibre-like texture produced by intermediate hammering. Thus, in our opinion, the analysis of the texture by ND can be a useful datum for archaeometallurgical characterization, but it should not be considered as a stand-alone method, since it could provide partial or misleading information. Rather, all of the TOF-ND characterization techniques reported here should be suitably applied, and integrated with elemental characterization techniques for a thorough investigation.

In conclusion, we have carried out the first documented analytical investigation on the Picenum bronze collection exhibited at the Marches National Museum of Archaeology, in a non-destructive way. Previously developed TOF-ND techniques, including phase and microstructural analyses, along with a new approach based on residual stress measurements by the ENGIN-X diffractometer, were successfully applied here to determine the composition and the

working process data. The analysis of the alloy composition by phase and tin quantification, along with microstructural information provided by peak shape analysis and the mapping of microstrains, allowed the derivation of a fairly complete technological description. We also discussed the potential of texture analysis through measurements on standard samples and two ancient objects, since the acquisition of reliable experimental pole figures was not possible for the set of objects investigated here, due to their complex shapes.

From the archaeometallurgical standpoint, at the present preliminary stage of the investigation on the bronzes from the Museum collection, we have found relationships with known features of Etruscan production. Further studies will be carried out in the near future in order to better document these relationships, as well as to determine any eventual differences and autonomous technological development.

ACKNOWLEDGEMENTS

The authors wish to thank Dr G. Baldelli of the Soprintendenza per i Beni Archeologici delle Marche, Ancona, for having provided archaeological data on the objects from the Marches National Museum of Archaeology that we investigated; P. Fabiani and Dr F. Milazzo, of the same institution, for the radiographic investigations; and Dr L. Lutterotti, of the Università di Trento, for having provided useful information on the use of the code MAUD that he developed.

REFERENCES

Allen, A. J., Andreani, C., Hutchings, M. T., and Windsor, C. G., 1985, Neutron diffraction methods for the study of residual stress fields, *Advances in Physics*, **34**, 445–73.

Artioli, G., Dugnani, M., Hansen, T., Lutterotti, L., Pedrotti, A., and Sperl, G., 2003, Crystallographic texture analysis of the iceman and coeval copper axes by non-invasive neutron powder diffraction, in *Die Gletschermumie aus der Kupferzeit 2* (ed. A. Fleckinger), 9–22, Museo archeologico del'Alto Adige, Bolzano.

Babbi, A., 2003, Le fibule della raccolta comunale di Tarquinia: alcune considerazioni tecnologiche, in *Fibulae* (ed. E. Formigli), 59–74, Edizioni Polistampa, Firenze.

Cateni, G., 1995, *Corpus speculorum Etruscorum*, Volterra Museo Guarnacci, 1, 'L'Erma' di Bretschneider, Roma.

Coppola, R., Lapp, A., Magnani, M., and Valli, M., 2002, Small angle neutron scattering investigation of microporosity in marbles, *Applied Physics A*, **74**, S1066–8.

Craddock, P. T., 1986, The metallurgy and composition of Etruscan bronze, *Studi Etruschi*, **52**, 211–71.

Dann, J. A., Daymond, M. R., Edwards, L., James, J., and Santisteban, J. R., 2004, A comparison between ENGIN and ENGIN-X, a new diffractometer optimized for stress measurement, *Physica B*, **350**, 511–14.

Daymond, M. R., Bourke, M. A. M., Von Dreele, R. B., Clausen, B., and Lorentzen, T., 1997, Use of Rietveld refinement for elastic microstrain determination and for evaluation of plastic strain history from diffraction spectra, *Journal of Applied Physics*, **82**, 1554–62.

Del Francia, P. R., 1998, La Lupa, in *Appunti di restauro*, 19–52, Soprintendenza Archeologica dell Toscana, Firenze.

Giachetti, R. Giorgetti, F., Miccio, M., Pecchioli, R., and Ronchi, M., 1984, Relazione sulle analisi, in *Due Bronzi di Riace, rinvenimento, restauro, analisi ed ipotesi attributive* (ed. P. R. Del Francia), 85–105, Istituto Poligrafico e Zecca dello Stato, Roma.

Humphreys, F. J., and Hatherly, M., 1996, *Recrystalization and related annealing phenomena*, Elsevier Science, Oxford.

Kockelmann, W., Kirfel, A., and Haehnel, E., 2001, Non-destructive phase analysis of archaeological ceramics using TOF neutron diffraction, *Journal of Archaeological Science*, **28**, 213–22.

Kockelmann, W., Pantos, E., and Kirfel, A., 2000, Neutron and synchrotron radiation studies of archaeological objects, in *Radiation in art and archaeometry* (eds. D. C. Creagh and D. Bradley), 347–77, Elsevier, Amsterdam.

Kocks, U. F., Tomé, C. N., and Wenk, H.-R., 1998, *Texture and anisotropy*, Cambridge University Press, Cambridge.

Larson, A. C., and Von Dreele, R. B., 1986, *GSAS, General Structure Analysis System*, Report LAUR86-748, Los Alamos National Laboratory, New Mexico.

Lutterotti, L., Matthies, S., and Wenk, H. R., 1999, MAUD (Material Analysis Using Diffraction): a user friendly Java program for Rietveld Texture Analysis and more, in *Proceedings of the 12th International Conference on Texture of Materials* (ed. J. A. Szpunar), vol. 1, 1599–610, NRC Research Press, Ottawa.

Pawley, G. S., 1981, Unit-cell refinement from powder diffraction scans, *Journal of Applied Crystallography*, **14**, 357–61.

Pecchioli, R., Giorgetti, F., Miccio, M., and Pallecchi, P. 1989, Indagini sul lampadario etrusco di Cortona, *Studi Etruschi*, **LV** (serie III), 245–8.

Riederer, J., 1999, Die metallanalyse der objekte aus kupferlegierungen, in Jurgeit, F., *Die etruskiscen und italischen Bronzen sowie Gegenstände aus Eisen, Blei und Leder im Badischen Landesmuseum Karlsruhe*, 297–343, Istituti Editoriali e Poligrafici Internazionali, Pisa.

Rietveld, H. M., 1969, A profile refinement method for nuclear and magnetic structures, *Journal of Applied Crystallography*, **2**, 65–71.

Rossi, M., 2003, Analisi di una fibula in bronzo mediante tomografia computerizzata, in *Fibulae* (ed. E. Formigli), 59–74, Edizioni Polistampa, Firenze.

Santisteban, J. R., Edwards, L., Steuwer, A., and Withers, P. J., 2001, Time-of-flight neutron transmission diffraction, *Journal of Applied Crystallography*, **34**, 289–97.

Santisteban, J. R., Edwards, L., Fitzpatrick, M. E., Steuwer, A., Withers, P. J., Daymond, M. R., Johnson, M. W., Rhodes, N., and Schooneveld, E. M., 2002, Strain imaging by Bragg edge neutron transmission, *Nuclear Instruments and Methods in Physic Research Section A*, **481**, 255–8.

Siano, S., Bartoli, L., Kockelmann, W., Zoppi, M., and Miccio M., 2004, 'Neutron metallography' of archaeological bronzes, *Physica B*, **350**, 123–6.

Siano, S., Bartoli, L., Zoppi, M., Kockelmann, W., Daymond, M., Dann, J. A., Garagnani G., and Miccio, M., 2003, Microstructural bronze characterisation by time of flight neutron diffraction, in *Proceedings of the International Conference 'Archaeometallurgy in Europe'*, vol. 2, 319–29, Associazione Italiana di Metallurgia, Milano.

Siano, S., Kockelmann, W., Zoppi, M., Miccio, M., Iozzo, M., Bafile, U., Salimbeni, R., Pini R., Celli, M., and Moze, O., 2002, Quantitative multiphase analysis of archaeological bronzes by neutron diffraction, *Applied Physics A*, **74**, **S**1139–42.

Von Dreele, R. B., Jorgensen, J. D., and Windsor, C. G., 1982, Rietveld refinement with spallation neutron powder diffraction data, *Journal of Applied Crystallography*, **15**, 581–9.

Wenk, H. R., and Van Houtte, P., 2004, Texture and anisotropy, *Reports on Progress in Physics*, **67**, 1367–428.

Yanxia, X., Lutterotti, L., Wenk H. R., and Kovacs, F., 2004, Texture analysis of ancient coins with TOF neutron diffraction, *Journal of Materials Science*, **39**, 3329–37.